

SCIENCES

GEOSCIENCE

Dynamics of the Continental Lithosphere

**Fission-track
Thermochronology**

*Methodology and Applications
to Geology*

**Coordinated by
Marc Jolivet**

ISTE

WILEY

Table of Contents

[Cover](#)

[Table of Contents](#)

[Title Page](#)

[Copyright Page](#)

[Introduction](#)

[1 Introduction to Detrital Apatite and Zircon Fission-track Thermochronology](#)

[1.1. Introduction](#)

[1.2. Principals of fission-track dating](#)

[1.3. Sample preparation and fission-track dating](#)

[1.4. Statistics of fission-track dating](#)

[1.5. Detrital thermochronology](#)

[1.6. Applications of detrital thermochronology](#)

[1.7. Concluding remarks](#)

[1.8. References](#)

[2 Thermal History Modeling for Thermochronology](#)

[2.1. Introduction](#)

[2.2. Modeling diffusion and annealing](#)

[2.3. Thermal history modeling](#)

[2.4. Summary](#)

[2.5. References](#)

[3 LA-ICP-MS \$^{238}\text{U}\$ Determination for Fission-track Dating](#)

[3.1. Introduction](#)

[3.2. Zeta approach for LA-ICPMS](#)

3.3. Absolute versus relative determination of U concentration

3.4. Statistical data processing

3.5. Sample preparation and data acquisition for LA-ICP-MS dating

3.6. Comparison of EDM and LA-ICP-MS methods

3.7. Conclusion

3.8. References

4 (U-Th-(Sm))/He Thermochronometry and Chronometry: Principles, Applications and Limits

4.1. Introduction

4.2. Principle of the (U-Th-(Sm))/He

4.3. Analytical methods (U-Th-(Sm))/He and $^4\text{He}/^3\text{He}$

4.4. (U-Th-(Sm))/He and $^4\text{He}/^3\text{He}$ methods on various minerals

4.5. Examples of geological applications

4.6. Limitations

4.7. Acknowledgments

4.8. References

5 Application of Low-Temperature Thermochronology to the Dating and Quantification of Tectonic Movements: The Example of Asia

5.1. Introduction

5.2. A few reminders of the principles of fission-track thermochronology

5.3. The contribution of fission tracks to understanding the India-Asia collision

5.4. Conclusion

5.5. References

[Conclusion](#)

[List of Authors](#)

[Index](#)

[End User License Agreement](#)

List of Tables

Chapter 1

[Table 1.1. Decay constants and half-lives of U and Th isotopes. Note: \$\alpha\$ for \$\alpha\$ -...](#)

[Table 1.2. Activation energies and diffusion parameters for apatite and zircon...](#)

[Table 1.3. Commonly used fission-track age standards and dosimeter glasses](#)

Chapter 4

[Table 4.1. U, Th and Sm radioactivity and daughter products, with the average ...](#)

[Table 4.2. Average stopping distance of alphas for various minerals, according...](#)

[Table 4.3. Criteria and information to be obtained when selecting minerals for...](#)

[Table 4.4. U, Th and Sm concentration and diffusion coefficient for different ...](#)

List of Illustrations

Introduction

[Figure I.1. Portraits of Aristotle, James Ussher \(by P. Lely\), John William St...](#)

[Figure I.2. Main geochronometers and thermochronometers used and their tempera...](#)

[Figure I.3. Example of a cooling curve drawn by assembling temperature-age poi...](#)

[Figure I.4. Images of fission tracks in various minerals. From top to bottom a...](#)

Chapter 1

[Figure 1.1. Overview of the temperature sensitivity range of selected isotopic...](#)

[Figure 1.2. \(A\) \$^{238}\text{U}\$ - \$^{206}\text{Pb}\$ decay chain, with a series of eight \$\alpha\$ -decay steps a...](#)

[Figure 1.3. \(A\) Closure temperature concept \(modified after Braun et al. 2006\)...](#)

[Figure 1.4. \(A\) Partial annealing zone concept of decreasing apparent fission-...](#)

[Figure 1.5. Comparison of the partial annealing zone temperature ranges for fi...](#)

[Figure 1.6. Sampling of modern river sediments for detrital fission-track stud...](#)

[Figure 1.7. Mounting for fission-track analysis of \(A\) apatite grains in cold ...](#)

[Figure 1.8. Examples of well-etched \(A\) apatite and \(B\) zircon crystals mounte...](#)

[Figure 1.9. \(A\) Grain mount polishing and \(B\) etching procedures for apatite a...](#)

[Figure 1.10. Zircon fission-track age versus U content in relation to etch tim...](#)

[Figure 1.11. External detector method: \(A\) mounting of external mica detector ...](#)

[Figure 1.12. \(A\) Schematic sketch of polished apatite grain with etch pits, se...](#)

[Figure 1.13. Track lengths distributions and thermal histories \(after Gallaghe...](#)

[Figure 1.14. Example of high and low track count areas within one zircon grain...](#)

[Figure 1.15. Example for data presentation of detrital fission-track data, her...](#)

[Figure 1.16. Radial plot of the Rhone delta zircon fission-track data with \(A\)...](#)

[Figure 1.17. \(A\) Lag-time concept \(modified from Bernet \(2019\)\). \(B\) Potential...](#)

[Figure 1.18. \(A\) Radial plot with minimum age of the Isère River, France \(Bern...](#)

[Figure 1.19. \(A\) Map of the Eastern Cordillera in Colombia between Bogotá and ...](#)

[Figure 1.20. \(A and B\) Double-dating concept for provenance analysis for discr...](#)

[Figure 1.21. \(A\) Zircon fission-track age or lag-time versus exhumation rate o...](#)

[Figure 1.22. Detrital zircon fission-track central ages of modern river and Si...](#)

[Figure 1.23. \(A\) Simplified geological map of the Central and Eastern Himalaya...](#)

Chapter 2

[Figure 2.1. Typical ranges of closure temperature relevant to geological times...](#)

[Figure 2.2. An example of estimating diffusion parameters for He in apatite \(m...](#)

[Figure 2.3. \(A\) Predicted AHe and AFT ages, and \(B\) fission track length distr...](#)

[Figure 2.4. \(A\) Predicted AHe and AFT ages, and \(B\) fission track length distr...](#)

[Figure 2.5. Results of an inverse modeling run based on synthetic data produce...](#)

[Figure 2.6. As in Figure 2.5, but the inversion approach allowed more complex ...](#)

Chapter 3

[Figure 3.1. Schematic diagram of an LA-ICP-MS \(Claverie 2009\).](#)

[Figure 3.2. Theoretical example of a calibration curve. On the basis of repeat...](#)

[Figure 3.3. Example of a primary zeta factor determination session. Intra-crys...](#)

[Figure 3.4. Radial plots \(A\) principle of construction of a radial plot. The a...](#)

[Figure 3.5. \(A\) Example of a mount for LA-ICP-MS dating. \(B\) Example of an apa...](#)

Chapter 4

[Figure 4.1. Ejection of helium atoms upon emission for three parent atom distr...](#)

[Figure 4.2. Impact of alpha particle implantation during ejection into neighbo...](#)

[Figure 4.3. Apatite cell and He insertion sites. \(A\) Double mesh of an apatite...](#)

[Figure 4.4. He diffusion in fluorapatite at 500 K, adapted from Djimbi et al. ...](#)

[Figure 4.5. Shape of the helium profile inside a cylinder approximating an apa...](#)

[Figure 4.6. Arrhenius diagram obtained from diffusion experiments for fragment...](#)

[Figure 4.7. Field of closure temperatures \$T_c\$, for a cooling rate of \$10^\circ\text{C}/\text{My}\$, f...](#)

[Figure 4.8. Photographic plate of selected apatite \(left\) and zircon \(right\) c...](#)

[Figure 4.9. Schematic model of closure temperature evolution with dose. Blue: ...](#)

[Figure 4.10. Typical dispersion of AHe ages as a function of \(A\) effective ura...](#)

[Figure 4.11. Evolution of AHe ages as a function of effective uranium concentr...](#)

[Figure 4.12. Evolution of temperature of closure \$T_c\$ as a function of alpha dos...](#)

[Figure 4.13. Direct thermal model of ZHe data from two geological cases illust...](#)

[Figure 4.14. Schematic representation of the couplings involved in landform ev...](#)

[Figure 4.15. \(a\) Map of France with indication of the study area \(black rectan...](#)

[Figure 4.16. Regional synthesis of thermochronological results from the easter...](#)

[Figure 4.17. \(A\) Simplified geological map of the Western Alps \(Schwartz et al...](#)

[Figure 4.18. \(A\) Geological map of the northwest African margin centered on th...](#)

[Figure 4.19. Conceptual model illustrating structural evolution and rock exhum...](#)

[Figure 4.20. \(A\) Geological map of the Aegean Sea showing the main tectonic st...](#)

[Figure 4.21. \(a\) simplified geological map of the Pyrenees, adapted from Terno...](#)

Chapter 5

[Figure 5.1. Top: topographic map of Asia showing the major mountain ranges dis...](#)

[Figure 5.2. Simplified paleogeographic map of the Upper Cretaceous: in brown, ...](#)

[Figure 5.3. \(A\) Distribution of average fission-track ages on apatite as a fun...](#)

[Figure 5.4. Representative photographs of the two types of topography characte...](#)

[Figure 5.5. Geological and tectonic context of the Longmen Shan range to the e...](#)

[Figure 5.6. \(A\) Interpolation of apatite fission-track mean age data available...](#)

[Figure 5.7. Topography of the northern margin of the Tibetan plateau, bounded ...](#)

[Figure 5.8. \(A\) General topographic and structural map of the Tian Shan region...](#)

[Figure 5.9. Topographical and geological diagram of the central and northern p...](#)

[Figure 5.10. Altitudinal profiles and thermal models obtained on the Ih Bogd m...](#)

Chapter 6

[Figure C.1. Modeling of the effect of topography on the shape of closure tempe...](#)

Figure C.2. Example of multi-method analysis and dating of a topography in the...

SCIENCES

Geoscience, Field Director - Yves Lagabriele

Dynamics of the Continental Lithosphere,
Subject Head - Sylvie Leroy

Fission-track Thermochronology

Methodology and Applications to Geology

Coordinated by

Marc Jolivet

ISTE

WILEY

First published 2024 in Great Britain and the United States by ISTE Ltd and John Wiley & Sons, Inc.

Apart from any fair dealing for the purposes of research or private study, or criticism or review, as permitted under the Copyright, Designs and Patents Act 1988, this publication may only be reproduced, stored or transmitted, in any form or by any means, with the prior permission in writing of the publishers, or in the case of reprographic reproduction in accordance with the terms and licenses issued by the CLA. Enquiries concerning reproduction outside these terms should be sent to the publishers at the undermentioned address:

ISTE Ltd
27-37 St George's Road
London SW19 4EU
UK

www.iste.co.uk

John Wiley & Sons, Inc.
111 River Street
Hoboken, NJ 07030
USA

www.wiley.com

© ISTE Ltd 2024

The rights of Marc Jolivet to be identified as the author of this work have been asserted by him in accordance with the Copyright, Designs and Patents Act 1988.

Any opinions, findings, and conclusions or recommendations expressed in this material are those of the author(s), contributor(s) or editor(s) and do not necessarily reflect the views of ISTE Group.

Library of Congress Control Number: 2023952196

British Library Cataloguing-in-Publication Data
A CIP record for this book is available from the British Library
ISBN 978-1-78945-173-3

ERC code:
PE10 Earth System Science

*PE10_11 Geochemistry, crystal chemistry, isotope geochemistry,
thermodynamics*

PE10_12 Sedimentology, soil science, palaeontology, earth evolution

Introduction

Marc JOLIVET

CNRS, University of Rennes, France

The age, duration and speed of processes are essential parameters for most Earth science studies. For example, to describe the growth and subsequent dismantling of a mountain range, we need to date the emplacement of magmas, determine the age and speed of metamorphic processes, and measure the slip rates of faults and erosion.

The first attempts to determine the Earth's age date back to antiquity, with Aristotle (384–322 BCE) declaring that the Earth is eternal. This thesis lasted until the end of the Middle Ages, before giving way to attempts at calculation based on the Bible. The Irish archbishop J. Ussher (1581–1656) declared that the Earth was formed at Creation, at the beginning of the night before October 23 in the year 4004 of the Julian calendar. It was not until the beginning of the 20th century, following Henri Becquerel's discovery of radioactivity in 1896, that modern geochronology developed. Using radiogenic helium produced by the decay of radium, J.W. Strutt (Lord Rayleigh) was the first to provide an age greater than 1 billion years. However, his approach was largely biased by the fact that radiogenic helium is produced not only by the radioactive decay of radium, but also by that of many other elements such as thorium and uranium. In the 1950s, technical advances made during the Second World War, notably in mass spectrometry, enabled Patterson (1956) to show that meteorites and the Earth formed at the same time 4.55 billion years ago (± 70 million years) ([Figure I.1](#)).



Figure I.1. *Portraits of Aristotle, James Ussher (by P. Lely), John William Strutt (Lord Rayleigh) and Clair C. Patterson.*

From this period onwards, a whole series of geochronological methods were developed based on the “closure temperature” principle (see [Chapter 1](#)). Every geochronological system consists of a mineral and a radioactive element–radiogenic element pair. The closure temperature corresponds to the temperature below which

diffusion of the radioactive and radiogenic isotopes in question is no longer sufficient to allow exchanges with the outside of the mineral (Dodson 1973). Geochronological methods therefore exist to date a wide range of geological phenomena over a wide range of temperatures, providing information in the form of an age associated with a temperature ([Figure 1.2](#)). The combined use of several geochronometers on a sample of the same rock enables us to follow the cooling history of this rock “in dotted lines”, highlighting periods of accelerated cooling, synonymous with tectonic movements ([Figure 1.3](#)).

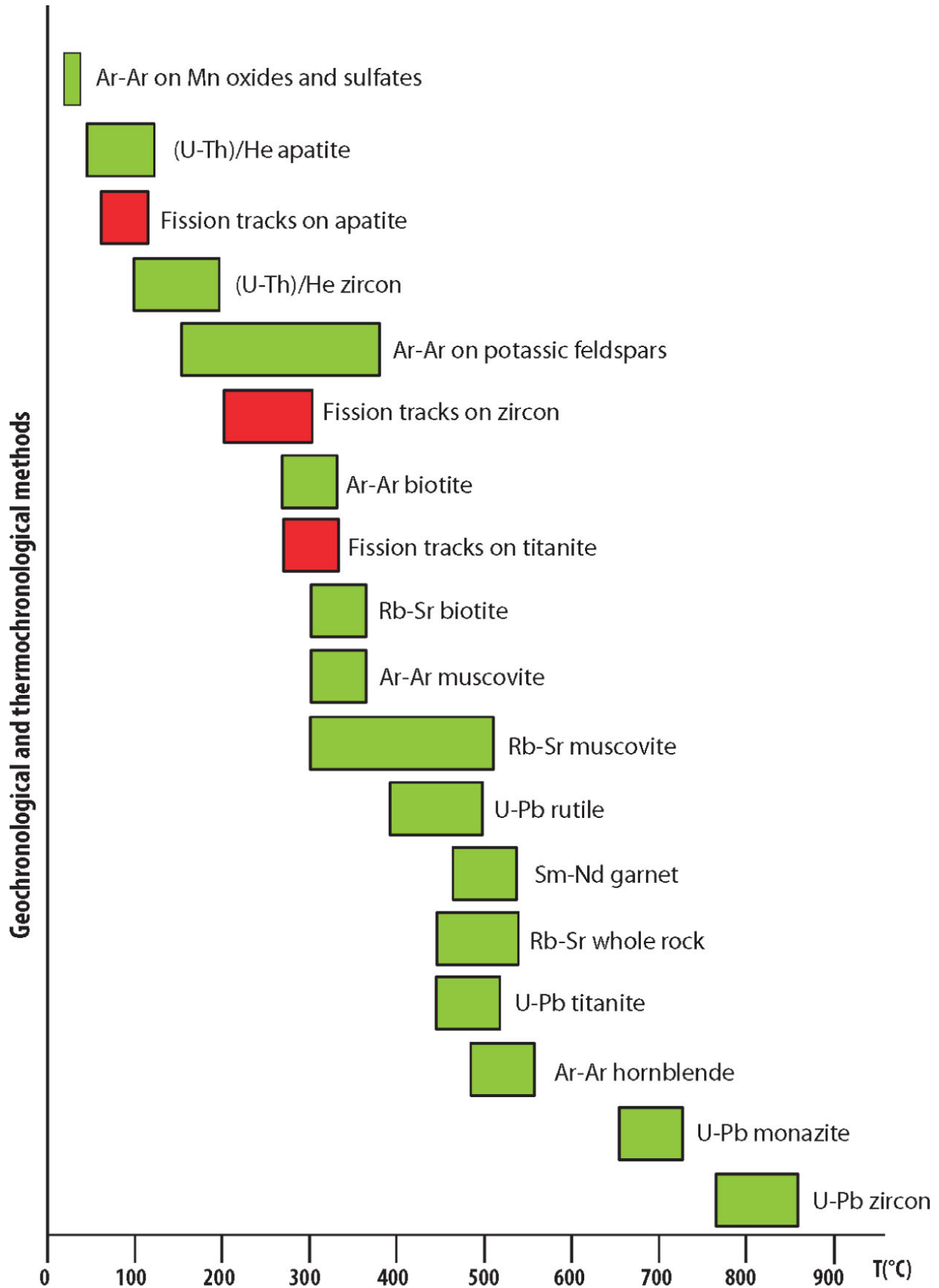


Figure 1.2. Main geochronometers and thermochronometers used and their temperature of application. Methods based on fission tracks are shown in red.

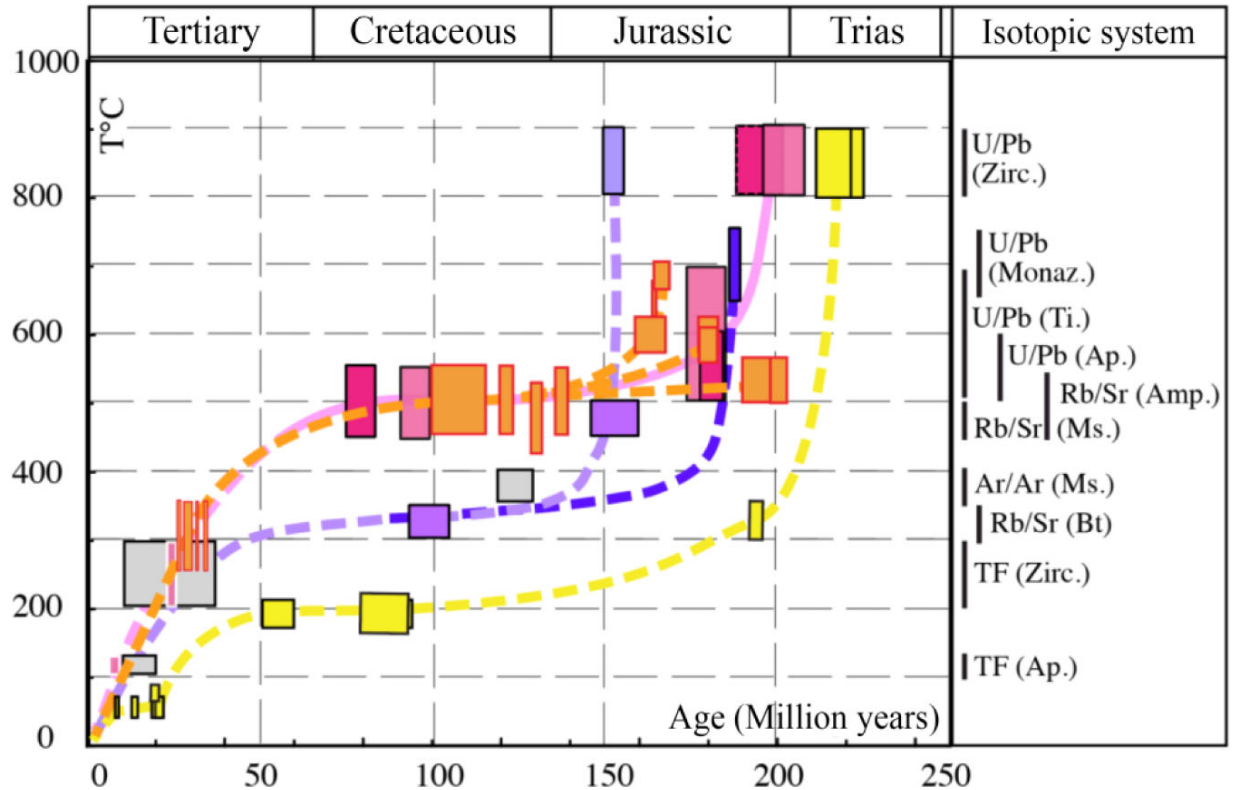


Figure 1.3. Example of a cooling curve drawn by assembling temperature-age points obtained from several geochronometers applied to the same sample. The thermal history obtained is discontinuous. Modified from Roger et al. (2011).

In 1958, D.A. Young discovered that LiF crystals coated with a uranium film and irradiated with thermal neutrons showed a number of “holes” after chemical treatment. The number of these “holes” is in perfect agreement with the theoretical number of fission fragments of uranium atoms expected for the neutron dose applied (Young 1958). In fact, the spontaneous fission of an atom of ^{238}U or ^{232}Th generates two ionizing particles which, as they pass

through a solid medium, leave a “track”. In a crystallized solid, this “track” corresponds to the displacement of atoms in the crystal lattice. In an organic medium such as plastic, the track materializes as chains of broken molecules (Durani and Bull 1987). In the early 1960s, R.L. Fleischer, P.B. Price and R.M. Walker developed a method for detecting these “fission tracks”, adapting Young’s technique for revealing tracks by chemical etching to a wide variety of materials (minerals, glass, plastics) (Fleischer et al. 1965, 1975) ([Figure I.4](#)). As the number of fission tracks in a given mineral depends directly on the concentration of radioactive elements (mainly ^{238}U) and the time over which the mineral has accumulated tracks, it is possible to use this phenomenon as a geochronometer: measuring the concentration of ^{238}U and the density of fission tracks enables time to be calculated. Wagner (1968) demonstrated in 1968 that if minerals such as apatites or zircons are heated, the fission tracks they contain can be “erased” (the crystal lattice is reconstituted). The higher the temperature, the faster the tracks disappear. For each mineral, the temperature range in which the tracks disappear over a time scale compatible with geological time (a few million years to tens of millions of years) is called the partial annealing zone I (PAZ) of the tracks. In apatites, for example, it ranges from around 130°C to 60°C, and in zircons, it ranges from around 250°C to 180°C. Other parameters, such as pressure, have no appreciable effect on the rate at which tracks are erased (Fleischer et al. 1975). By measuring the distribution of track lengths in a mineral, it is then possible to statistically calculate a temperature-time path for each sample, making it possible to continuously monitor the thermal history of a sample in the PAZ temperature range (see [Chapter 2](#)).

Fission-track thermochronology has become a key tool in geological research, whether fundamental (tectonics,

geomorphology, sedimentology) or applied (hydrocarbon prospecting). In this book, we explore the latest methodological developments that are constantly improving the results obtained using this technique. The first chapter will first provide a general reminder of the principle behind the method, before detailing its application to detrital thermochronology. The second chapter deals with the statistical modeling of the thermal history of samples. The third chapter focuses on a brand-new technique for determining the ^{238}U concentration of a sample using in situ elemental analysis. The fourth chapter develops the (U-Th-(Sm))/He thermochronology method, based on the production of radiogenic He nuclei by the radioactive decay of uranium (^{235}U and ^{238}U), thorium (^{232}Th) and samarium (^{147}Sm). This method can be applied to the same minerals as the fission-track approach (essentially zircon and apatite) and covers very complementary temperature ranges from 50°C to 200°C (Ault et al. 2019; Gautheron and Zeitler 2020). Fission-track thermochronology and (U-Th-(Sm))/He are therefore often used together in geological studies. Finally, the last chapter proposes an application to geodynamics, explaining how fission-track thermochronology has been used to describe the thermal history of the Central Asian and Tibetan ranges in the context of the collision between the Indian and Asian continents.

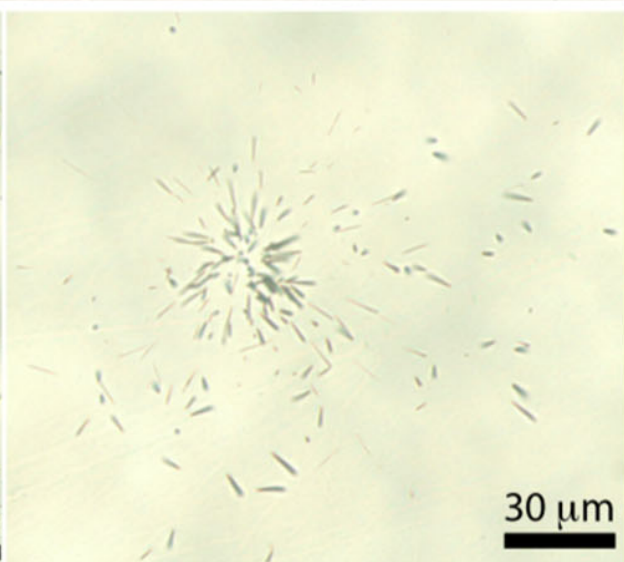
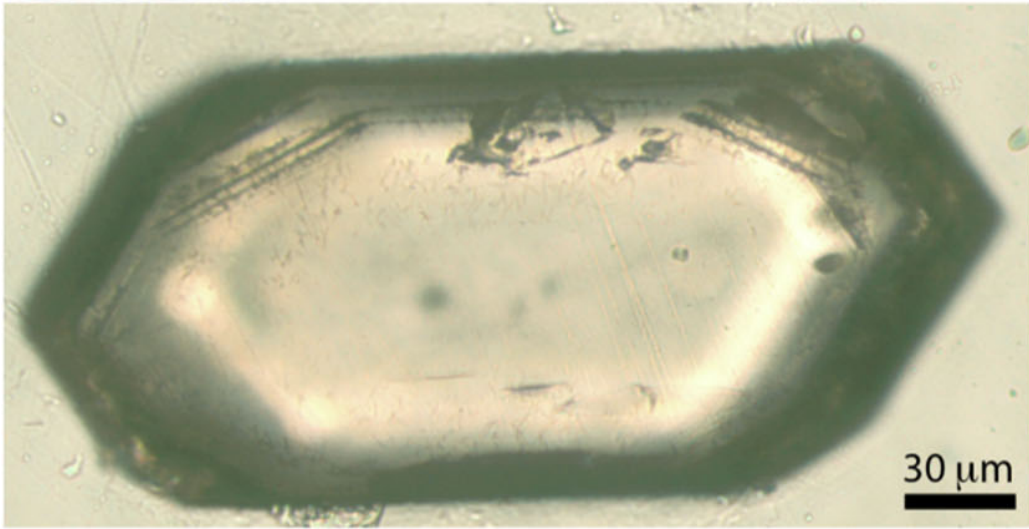
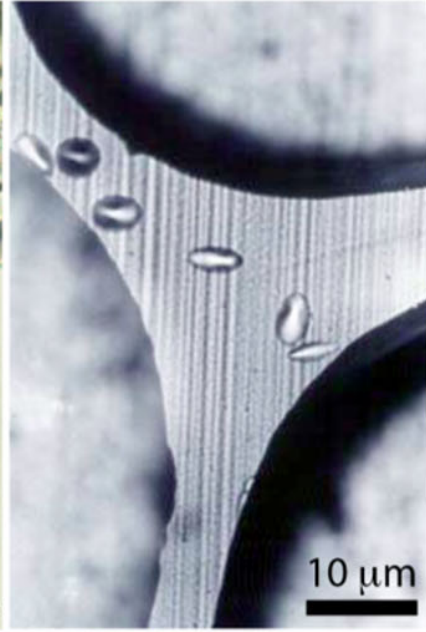
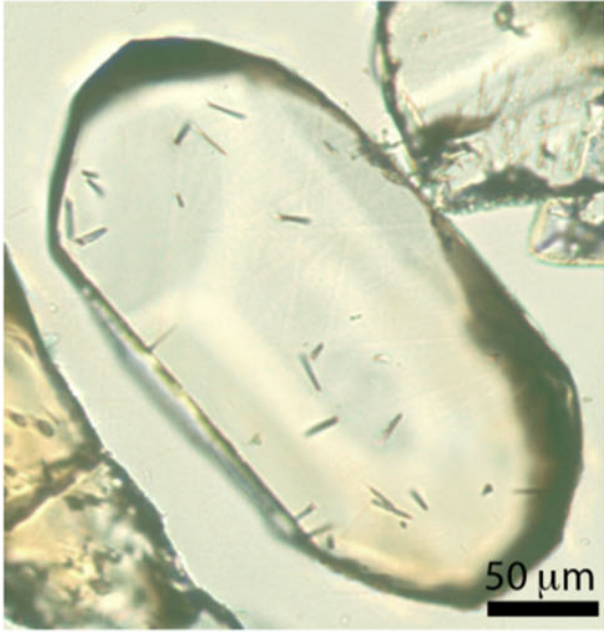


Figure I.4. *Images of fission tracks in various minerals. From top to bottom and left to right: apatite, glass, zircon (note the very small size and large number of these tracks), white micas (irradiated in contact with apatites) and white micas (irradiated in contact with an apatite containing a zircon whose very high relative uranium content has caused the high density of “star” tracks)*

References

- Ault, A.K., Gautheron, C., King, G.E. (2019). Innovations in (U-Th)/He, fission track, and trapped charge thermochronology with applications to earthquakes, weathering, surface-mantle connections, and the growth and decay of mountains. *Tectonics*, 38(11), 3705–3739. doi: 10.1029/2018TC 005312.
- Dodson, M.H. (1973). Closure temperature in cooling geochronological and petrological systems. *Contribution to Mineralogy and Petrology*, 40, 259–274.
- Durrani, S.A. and Bull, R.K. (1987). *Solid State Nuclear Track Detection: Principles, Methods and Applications*. Pergamon Books Ltd, Oxford.
- Fleischer, R.L., Price, P.B., Walker, R.M. (1965). The ion explosion spike mechanism for formation of charged particle tracks in solids. *Journal of Applied Physics*, 36, 3645–3652.
- Fleischer, R.L., Price, P.B., Walker, R.M. (1975). *Nuclear Tracks in Solids*. University of California Press, Berkeley.
- Gautheron, C. and Zeitler, P.K. (2020). Noble gases deliver cool dates from hot rocks. *Elements*, 16(5), 303–309. doi: 10.2138/gselements.16.5.303.

- Patterson, C. (1956). Age of meteorites and the Earth. *Geochimica et Cosmochimica Acta*, 10(4), 230-237.
- Roger, F., Jolivet, M., Cattin, R., Malavieille, J. (2011). Mesozoic-Cenozoic tectonothermal evolution of the eastern part of the Tibetan Plateau (Songpan-Garzê, Longmen Shan area): Insights from thermochronological data and simple thermal modeling. In *Growth and Collapse of the Tibetan Plateau*, Gloaguen, R. and Ratschbacher, L. (eds). Geological Society (Special Publication), London.
- Wagner, G.A. (1968). Fission-track dating of apatite. *Earth and Planetary Science Letters*, 4, 411-415.
- Young, D.A. (1958). Etching of radiation damage in lithium fluoride. *Nature*, 182, 375-377.

1 Introduction to Detrital Apatite and Zircon Fission-track Thermochronology

Matthias BERNET

Institut des Sciences de la Terre, University Grenoble Alpes, France

Italienische Reise

Noch wunderlicher erschien ich diesem Begleiter, als ich auf allen seichten Stellen, deren der Fluß gar viele trocken läßt, nach Steinchen suchte und die verschiedenen Arten derselben mit mir fortrug. Ich konnte ihm abermals nicht erklären, daß man sich von einer gebirgigen Gegend nicht schneller einen Begriff machen kann, als wenn man die Gesteinsarten untersucht, die in den Bächen herabgeschoben werden, und daß hier auch die Aufgabe sei, durch Trümmer sich eine Vorstellung von jenen ewig klassischen Höhen des Erdaltertums zu verschaffen. Auch war meine Ausbeute aus diesem Flusse reich genug, ich brachte beinahe vierzig Stücke zusammen, welche sich freilich in wenige Rubriken unterordnen ließen.

Johann Wolfgang von Goethe, Palermo, 4 April 1787

1.1. Introduction

The use of detrital apatite and zircon fission-track and (U-Th)/He dating or white mica ^{40}Ar - ^{39}Ar dating of modern river and beach sediments or ancient sandstone is a common approach in sediment provenance, source rock exhumation and basin analysis studies. In this chapter, the focus is on detrital apatite and zircon fission-track dating. Both techniques are considered as low-temperature thermochronology dating techniques, with temperature sensitivities in the range of ~ 250 - 180°C for zircon and ~ 130 - 80°C for apatite in comparison to high-temperature dating techniques such as zircon or monazite U-Pb dating ([Figure 1.1](#)).

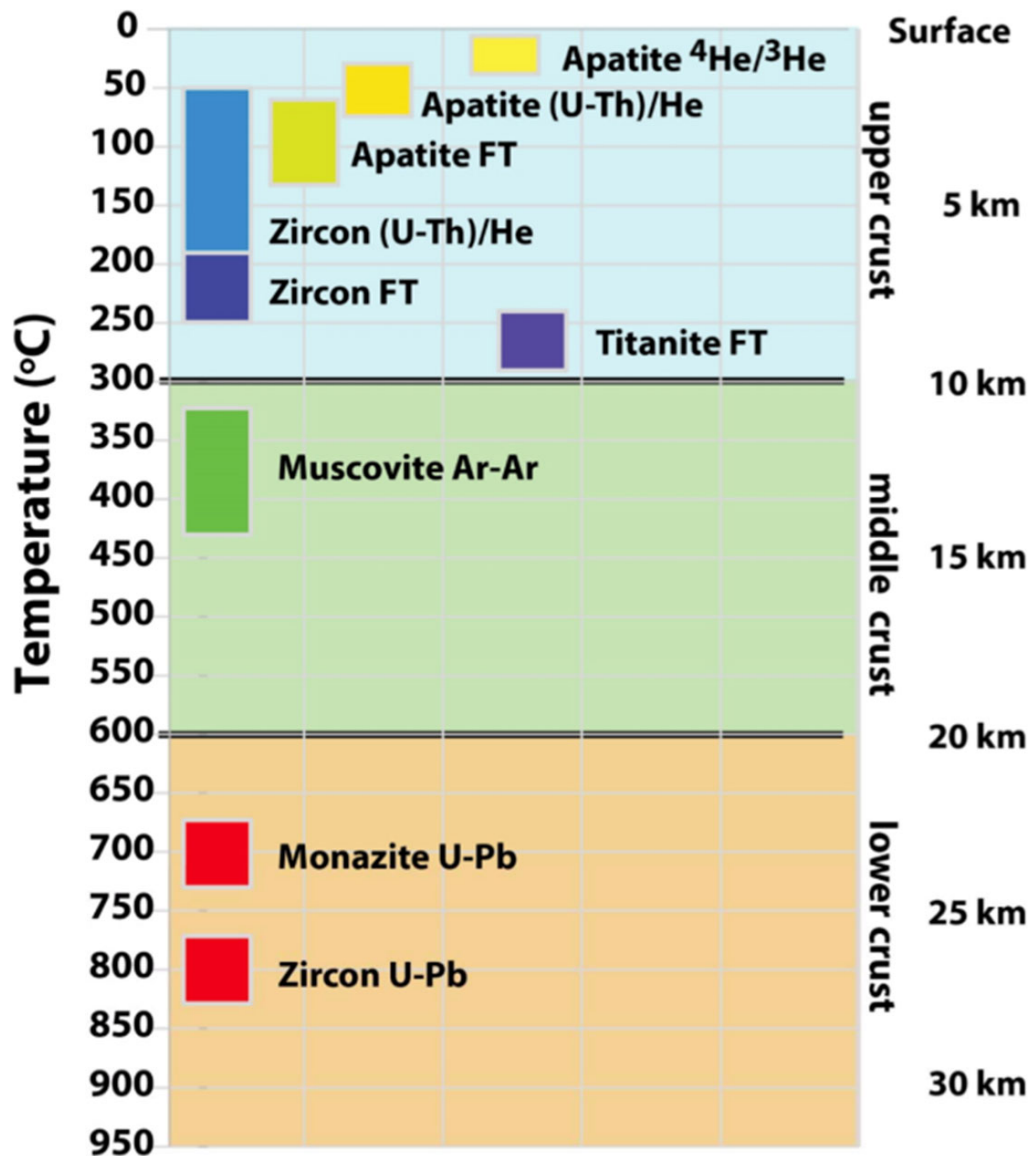


Figure 1.1. Overview of the temperature sensitivity range of selected isotopic dating techniques.

Apatite (density of 3.1–3.3 g/cm³) and zircon (density of 4.5–4.6 g/cm³) are heavy minerals in contrast to the density of quartz (2.65 g/cm³). Despite the highly variable apatite and zircon fertility of many upper crustal plutonic, volcanic and metamorphic rocks, both apatite and zircon are relatively common accessory minerals in many sand-sized clastic sediments and sedimentary rocks (Malusà and Garzanti 2019). Although apatite is susceptible to dissolution in acid depositional environments (e.g. bogs) or soils, and abrasion during fluvial transport, zircon is considered as ultra-stable, as long as the grains have not accumulated too much α -radiation damage and are metamict (Malusà and Garzanti 2019; Malusà and Fitzgerald 2020). Both minerals are chemically stable under diagenetic conditions during burial in sedimentary basins or during basin inversion and exhumation.

Since the first detrital zircon fission-track analysis studies in the 1980s (e.g. Hurford et al. 1984; Cervený et al. 1988), detrital apatite and zircon fission-track dating have developed into standard techniques that have been applied successfully to many different

decay, [93](#)

alpha-, [7](#), [71](#)

fission-, [27](#)

detrital grains, [7](#), [13](#), [31](#), [32](#)

diffusion, [6](#), [65](#), [66](#), [121](#), [128](#), [144](#)

domain, [132](#)

dosimeter, [20](#), [22](#), [28](#)

Durango, [21](#), [25](#), [28](#), [69](#), [105](#), [113](#), [143](#)

E, F

ejection, [69](#), [137](#)

erosion, [112](#), [155](#), [197](#), [206](#), [209](#)

exhumation, [2](#), [26](#), [32](#), [34](#), [36](#), [43](#), [145](#), [150](#), [188](#), [190](#), [194](#), [205](#), [209](#)

external

detector, [3](#), [20](#), [28](#), [94](#), [111](#), [113](#)

standard, [99](#)

fault, [162](#), [188](#), [200](#)

F_T , [126](#), [137](#), [139](#)

Fish Canyon Tuff, [21](#), [28](#)

fission tracks, [1](#), [69](#), [93](#)

confined tracks, [23](#)

Dpar, [24](#), [25](#)

induced tracks, [94](#)

spontaneous fission, [93](#)